Towards All Carbon Solar Cells

2013 GCEP Report - External

Investigators

Zhenan Bao, Professor, Chemical Engineering

Michael Vosgueritchian, Graduate Researcher

Huiliang Wang, Graduate Researcher

Ghada Koleilat, Postdoctoral Researcher

Nan Liu, Postdoctoral Researcher

Myung Gil Kim, Postdoctoral Researcher

Abstract

Herein we describe our work toward an efficient solar cell made in its entirety with carbon based materials. The different arrangements and combinations in which carbon can exist produce a wide variety of compounds that have unique physical, chemical and electrical properties. Some of these allotropes behave as conductors while others are classified as semiconducting. Our efforts focus on taking advantage of the carbon based materials' potential and optimally employ them together to form an all carbon solar cell. We first briefly discuss our recent publication on a first demonstration of an all carbon solar cell employing single walled carbon nanotubes (SWNTs) in conjunction with fullerenes as the active junction, and single walled carbon nanotubes and graphene oxide as the electrodes. We will then report on ongoing work towards engineering a much more efficient solar cell which include optimizing material processing specifically the sorting of semiconducting SWNTs of various diameters as well as moving towards the formation of an interpenetrating bulk heterojunction of the donor and acceptor layers. We will also report on our work regarding the careful controlling of the doping of the graphitic electrodes via a range of techniques to enable efficient extraction of both hole and electrons in a solar cell.

Content

1 All Carbon Solar Cell

1.1 First Reported Demonstration of an all Carbon Solar Cell *(Ramuz et al. ACS Nano 2012)*

Carbon is among the oldest elements discovered and one of the most abundant in the earth's crust. The processing of the different allotropes of carbon can potentially be mass produced easily at low cost. In addition, these materials can be dispersed in solution enabling roll-roll deposition processes that is attractive to large scale flexible electronics applications. Due to the exceptional electrical and optical properties of these materials, we employ them in a unique combination to form the first demonstration of an all carbon solar cell. Our structure, shown in Figure 1, is composed of a bilayer film of a solution sorted semiconducting SWNTs as the donor and C_{60} as the acceptor. Our demonstration focused on comparing the performance of the carbon solar cell employing standard electrodes with appropriately doped carbon electrodes.

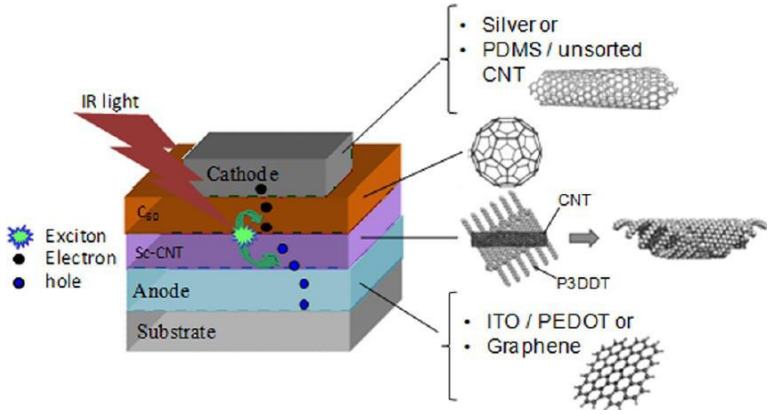

Figure 1 Structure of an all carbon solar cell

We reported on our efforts on replacing the ITO anode with reduced graphene oxide (rGO) layers and the top reflective metallic Ag cathode with n-type doped SWNT films. With the use of these carbon based electrodes, we demonstrated the first all-carbon based solar cell.

Active Layer Structure

The semiconducting high-pressure carbon monoxide (HiPco) SWNTs employed as in the active layer were sorted using the organic semiconducting polymer regioregular Poly(3-dodecylthiophene-2,5-diyl) (P3DDT) as described in our 2011 report published in Nature Communications by Lee *et al*. Essentially, the long chained thiophene polymer selectively "wraps" around semiconducting SWNTs resulting in a well dispersed s-SWNTs solution void of metallic SWNTS. The sorted SWNTs solutions and deposited films absorb in the infrared region up to 1500 nm as shown in Figure 2.

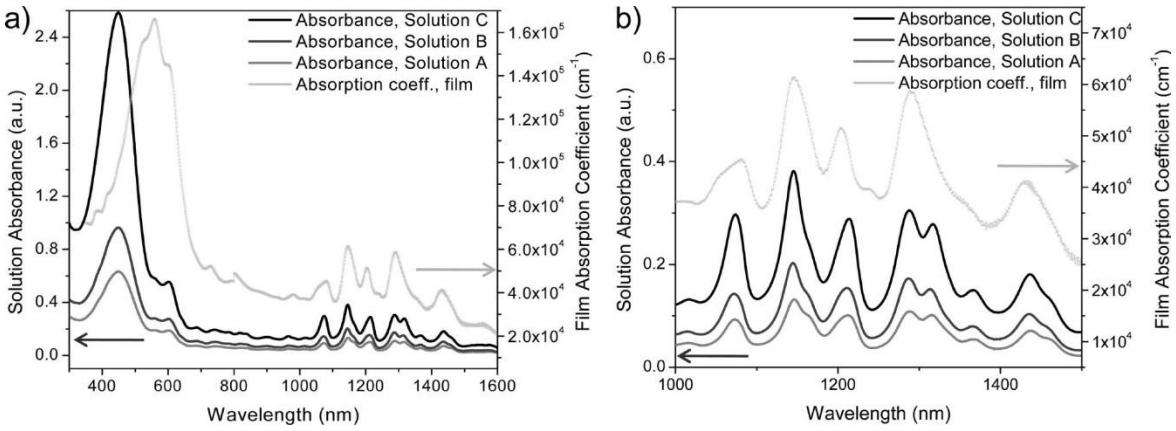

Figure 2 Absorption spectra of solutions and films of P3DDT sorted HiPco SWNTs

The absorption range of SWNTs is highly dependent on the diameter and chirality of the SWNTs, which is pre-determined by the SWNT synthesis and sorting process. One advantage to incorporating a broad range of tube chiralities as in our case is to increase the potential number of photons that can be absorbed and thus the current density that can be generated in a solar cell.

As shown in Figure 1, the sorted HiPco SWNTs formed a bilayer junction with the C60. The latter was thermally evaporated on top of the SWNTs network to form a continuous homogenous layer as show in Figure 3.

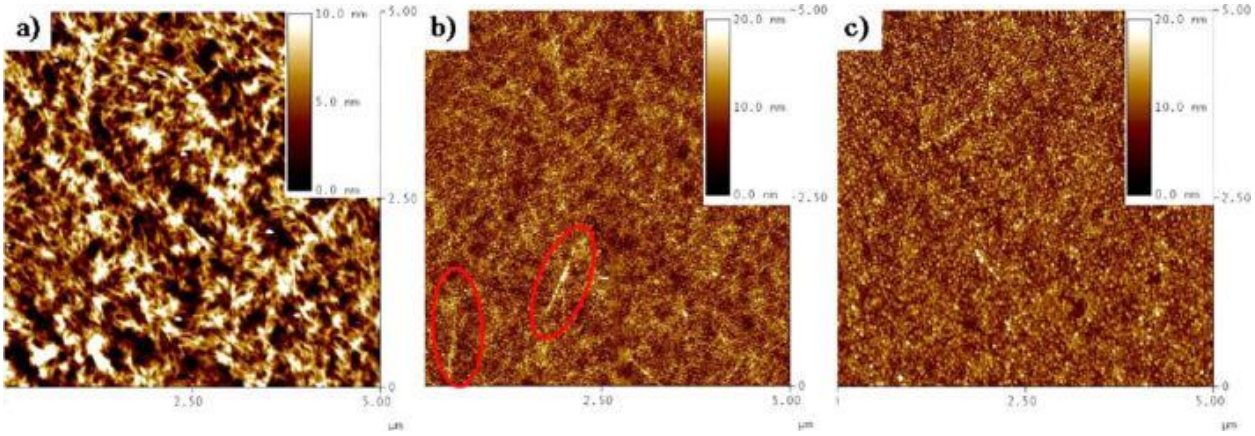

Figure 3 (a) Sorted SWNTS network (b) thin film of C60 deposited on top showing protruding SWNTs (c) thick C60 film resulting in a complete coverage of the SWNTs network.

The following tables summarize the device performance of our carbon active solar cell with under various processing and illumination conditions. The near-infrared (NIR) performance allows us to isolate the contribution of the infrared sensitive SWNTs in the device.

TABLE 1. PV Characteristics for Devices with Different SWNT Concentrations for NIR Illumination and under Standard Illumination AM1.5 100 mW/cm^2 [a]

	NIR illumination						AM1.5	
solution	J_{sc} (mA/cm^2)	V_{oc} (V)	FF	on/off @ 0 V	av PCE (%)	max PCE (%)	av PCE (%)	max PCE (%)
solution A	-2.29×10^{-2}	0.28	0.403	480	5.62×10^{-3}	6.35×10^{-3}	2.28×10^{-1}	2.40×10^{-1}
solution B	-6.20×10^{-2}	0.29	0.436	1996	1.73×10^{-2}	2.04×10^{-2}	2.34×10^{-1}	2.38×10^{-1}
solution C	-1.13×10^{-1}	0.29	0.348	3180	2.54×10^{-2}	2.79×10^{-2}	1.80×10^{-1}	1.84×10^{-1}

[a] The data correspond to five devices per solution.

TABLE 2. PV Characteristics of a Device Made with Different Deposition Conditions with Solution C (30 mg/25 mL) for NIR Illumination and under Standard Illumination AM1.5 100 mW/cm^2 [a]

	NIR illumination						AM1.5	
deposition/thickness	J_{sc} (mA/cm^2)	V_{oc} (V)	FF	on/off @ 0 V	av PCE (%)	max PCE (%)	av PCE (%)	max PCE (%)
spin coat 1×/3 nm	-9.92×10^{-2}	0.30	0.43	2395	2.85×10^{-3}	3.82×10^{-2}	0.184	0.191
spin coat 3×/3 nm	-1.29×10^{-1}	0.31	0.41	2707	3.65×10^{-2}	2.04×10^{-2}	0.174	0.177
spin coat 5×/3 nm	-1.48×10^{-1}	0.30	0.40	3054	4.00×10^{-2}	4.32×10^{-2}	0.175	0.179
drop cast/25—100 nm	-1.41×10^{-1}	0.30	0.39	18910	3.56×10^{-2}	4.24×10^{-2}	0.125	0.140

[a] The data correspond to five devices per deposition condition with a 140 nm C_{60} layer.

One of the main determinant of the junction efficiency is the alignment of the donor and acceptor's lowest unoccupied molecular orbital (LUMO) and highest occupied molecular orbital (HOMO) levels. In an ideal case, the donor and acceptor in the system form a type II heterojunction where the donor's LUMO is slightly above the acceptor's with their difference exceeding the exciton binding energy as shown in Figure 4 (a). However, our structure's band diagram is far from ideal and suffers from two major limitations. To start with, not all the sorted HiPco SWNTs chiralities form a type II with the C60 which means that a significant amount of excitons cannot be efficiently extracted. A second major obstacle is the P3DDT polymer "wrapping" around the majority of the SWNTs lengths thus preventing for the most part C60 of forming a direct junction with the SWNTs. The latter significantly increases the recombination losses within the solar cell. The real case energy band diagram is presented in Figure 4(b).

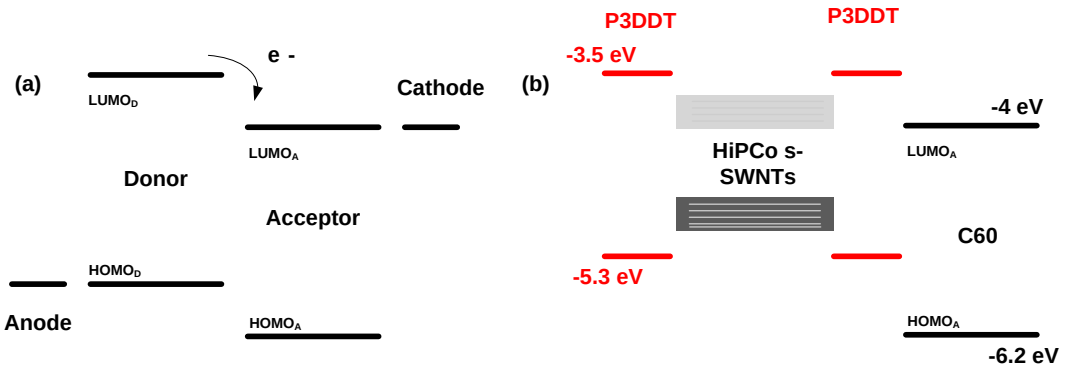

Figure 4 Energy band diagram of (a) ideal donor-acceptor bilayer (b) carbon solar cell

Carbon Based Electrodes

Reduced graphene oxide (rGO) anodes were fabricated using a thermal reduction method previously developed in our group by Becerril *et al.* (*ACS Nano 2008*). A graphene electrode was chosen due to the smooth films that can be formed, thus reducing the amount of leakage and the possibility of shorting in the device. To deepen the work-function of the rGO films, they were treated to short periods, 5 to 10 sec, of O_2 plasma, which resulted in a work-function increase from 4.9 eV to 5.3 eV. To evaluate the effectiveness of the rGO electrode, devices were fabricated with the rGO anode and the standard Ag

cathode. In addition to rGO anodes with plasma, devices were fabricated with an additional PEDOT smoothening layer. The photovoltaic performances for these devices are summarized in Table 3. As can be seen, the devices with rGO anode and Ag cathode resulted in decreased V_{oc} and FF compared to the ITO/PEDOT anode, with an associated decrease in the PCE. The reduced performance is attributed to the lower conductivity of the rGO compared to that of the ITO and the resulting increase in parasitic losses. Also, the device to device variation was significant. We attributed both these results to the increased roughness of the rGO.

TABLE 3. PV Characteristics of Devices Made with rGO Anodes with Ag Cathodes, ITO Anodes with n-Type-Doped SWNT Cathodes, and rGO Anodes with n-Type-Doped SWNT Cathodes, for NIR Illumination and under Standard Illumination AM1.5 100 mW/cm^2 [a]

	NIR illumination						AM1.5	
anode/cathode	J_{sc} (mA/cm^2)	V_{oc} (V)	FF	on/off @ 0 V	av PCE (%)	max PCE (%)	av PCE (%)	max PCE (%)
rGO-plasma/Ag	-2.84×10^{-2}	0.25	0.52	1731	8.16×10^{-3}	8.16×10^{-3}	1.41×10^{-1}	1.41×10^{-1}
rGO-PEDOT/Ag	-4.51×10^{-2}	0.26	0.50	1035	1.31×10^{-2}	2.01×10^{-2}	2.36×10^{-1}	2.69×10^{-1}
ITO/n-doped SWNTs	-2.79×10^{-1}	0.08	0.25	30	1.29×10^{-2}	1.46×10^{-2}	2.49×10^{-1}	3.04×10^{-1}
rGO-plasma/n-doped SWNTs	-3.00×10^{-2}	0.18	0.28	1607	3.42×10^{-3}	4.10×10^{-3}	4.71×10^{-3}	5.67×10^{-3}

[a] It should be noted that not all devices fabricated using rGO anodes were successful because of large graphitic-like particulates that were formed during the rGO film fabrication step. The data correspond to 1, 3, 3, and 3 devices for the different anode/cathode combinations from top to bottom.

The SWNT cathodes were fabricated by spray-coating a solution of SWNTs (1/3 metallic) dispersed in N-Methyl-2-pyrrolidone (NMP) on polydimethylsiloxane (PDMS) substrates. These films were then doped n-type using the molecular n-type dopant (4-(1,3-dimethyl-2,3-dihydro-1H-benzoimidazol-2-yl)phenyl)dimethylamine (N-DMBI). After completion, these films were laminated on the rGO/SWNT:P3DDT/C_{60} layers by pressing the films together. To evaluate the effect of the n-type doped SWNT cathode, it was laminated on devices fabricated on the standard ITO anode. Table 3 summarizes the performances of these devices. As can be seen, there was a significant decrease in the V_{oc} for these devices, and a marginal decrease in the FF and J_{sc}, which decreased the overall PCE. We attributed the large decrease in V_{oc} for the NIR range due to contact issues between the laminated SWNT cathode and the C_{60} because of the high roughness of the SWNT cathode.

As a final step in the reported work, all-carbon devices were fabricated using the rGO anodes and n-type doped SWNT cathodes. The device yield was low due to shorting or high leakage. We attributed this to roughness and contamination issues in the rGO films compounded by the lamination process of the high roughness n-type doped SWNT films. Nevertheless, working devices were fabricated with the all-carbon structure and the performance is reported in table 3.

1.2 Ongoing Work on the Active Layer and Cathode of the All Carbon Solar Cell

With the demonstration of the first all carbon solar cell, we are currently aiming to improve the overall performance of the solar cell to showcase its viability as a novel solar technology able to harvest the NIR spectrum of the solar irradiance as well as its visible region. To that end, we are mainly pursuing the following directions:

- Bulk heterojunction to surmount the short carrier diffusion limitation
- Smaller diameter seminconducting SWNTs for better energy level alignment and enhanced carrier extraction

2 Oxide Dopant for Carbon Nanotube Electrodes

Even though SWNTs have been employed as highly transparent conductive electrode, their bulk film conductivity is not as high as compared to that of the commonly used ITO, the highly conductive PEDOT:PSS, or even the metal (Cu, Ag, and Ag) nanowire meshes. The sorting process enhances the conductivity, but requires huge cost increase to separate out the metallic SWCNT from the as-synthesized mixture of both metallic and semiconducting SWNTs. Moreover, the significant contamination from the surfactant used either reduces the conductivity or requires additional surfactant removal process steps. To enhance the conductivity of the SWNTs mixture for transparent electrode applications, a stable and effective doping method is thus crucial. Previously, our group demonstrated such a doping mechanism

with the thermal activation of SWNTs with MoO_3 (Hellstrom *et al. Nano Letters 2012*). The 450^oC annealed SWNTs/MoO_3 composite shows 5-6 fold conductivity increase with significant p-type doping. The p-type doping was confirmed with a noticeable Raman G-peak shift of the MoO_3/SWNTs composite, from 1590 cm^{-1} for the pristine SWNTs to 1600 cm^{-1} for the doped composite. The doped SWNTs/MoO_3 was thermally robust up to 300^oC in ambient air and was stable for extended time (> 400 hours) under ambient conditions.

The success of MoO_3 comes from its deep work function value and intrinsically ambient stable nature as an oxide. However, the high activation temperature required hinders the direct application of this methodology onto flexible polymeric substrates. In addition, the SWNTs/MoO_3 composite is subject to degradation with oxidation at the high processing temperature. Fortunately, there is wide range of other oxide based compounds that could potentially be used as possible charge transfer dopants. We identified a few other oxides as strong candidates and we are currently testing them.

3 N-type Doping of Graphene

Graphene with its high charge carrier mobility and electrical conductivity is very attractive for carbon based electrode applications. Chemical vapor deposition (CVD) is one of the promising methods to prepare large-area and high-quality graphene films. However, transferred CVD-graphene exhibits very strong p-type behavior due to the inherent doping by oxygen and moisture both in CVD-growth and solution-transfer process, limiting its application in organic photovoltaics (OPV). To circumvent this problem, we used 2-(2-methoxyphenyl)-1,3-dimethyl-2,3-dihydro-1*H*-benzoimidazole (*o*-MeO-DMBI) as a strong n-type dopant for CVD grown graphene to effectively tune its electrical properties (Wei *et al. Nano Letters 2013*). It is found that the Dirac points can be tuned significantly by spin-coating *o*-MeO-DMBI solutions on the graphene sheets at different concentrations. The transport of graphene can be changed from p-type to ambipolar and finally to n-type, which improves the feasibility of graphene based electrodes in OPV.

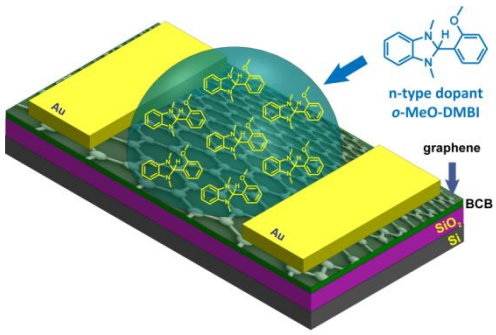

Figure 5. Chemical structure of *o*-MeO-DMBI and the schematic illustration of *o*-MeO-DMBI n-type doped CVD-grown graphene transistor by solution process.

To characterize the n-type doping effect of *o*-MeO-DMBI on graphene, we fabricated bottom-gate, top-contact CVD-grown graphene transistors as shown in Figure 5.

The electrical characteristics of as-transferred and doped CVD grown graphene transistors (Figure 6) were measured inside an N_2-filled glovebox. We compared the Dirac points, the gate dependence of maximum resistance, of various graphene transistors in order to investigate the n-type doping effect of *o*-MeO-DMBI. The as-transferred CVD graphene transistors exhibited a p-type transport behavior with highly positive Dirac points of ≥80 V (Figure 6a). Upon *o*-MeO-DMBI doping, the Dirac points of doped graphene transistors all shifted towards negative voltages, even when a very low solution concentration (0.01 mg/mL) of *o*-MeO-DMBI was used, indicating the strong n-type doping effect of *o*-MeO-DMBI on graphene sheets. With higher concentrations of *o*-MeO-DMBI solutions, all of the doped graphene transistors exhibited n-type transport behaviors with the Dirac points lower than -80 V. As shown in Figure 6c, after doping by 1 mg/ml o-MeO-DMBI chlorobenzene solution, the I_{ds} increased with the applied gate voltage from -80 V to 80 V (Vds = 0.1V). While in the as-transferred CVD graphene (Figure 6b), the $|I_{ds}|$ decreased with an increasing V_{gs} (V_{ds} = -0.1V), indicating the conversion of CVD graphene from p-type to n-type after doping. We note that with an *o*-MeO-DMBI solution concentration of 20 mg/mL, the resistivity of the n-type doped graphene (767 Ω/sq) was smaller than that of the as-transferred CVD graphene (850.6 Ω/sq) at V_{gs} = 0 V. This indicates that molecular n-type doping by o-MeO-DMBI could be also a promising approach for n-type conductors as transparent cathodes for solar cell.

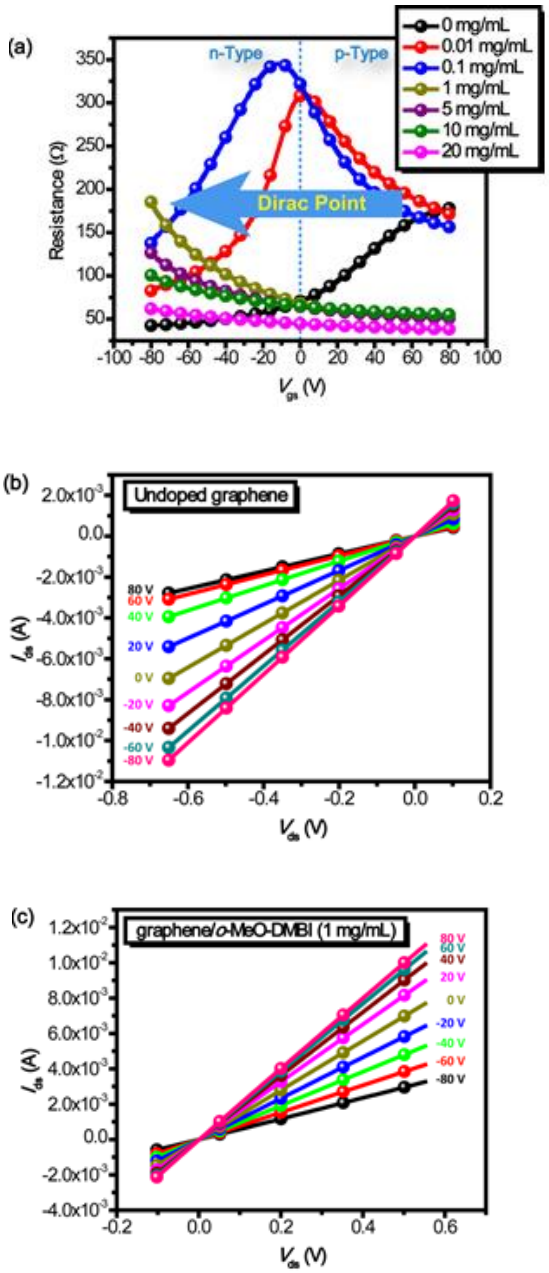

Figure 6 (a) Resistance of the as-transferred and doped CVD graphene transistors with various concentrations of *o*-MeO-DMBI solutions as a function of applied bottom gate voltages (V_{ds} = 0.1 V); (b) Output characteristics of the as-transferred CVD graphene transistor; (c) Output characteristics of the doped graphene transistor with *o*-MeO-DMBI solution concentration at 1 mg/mL.

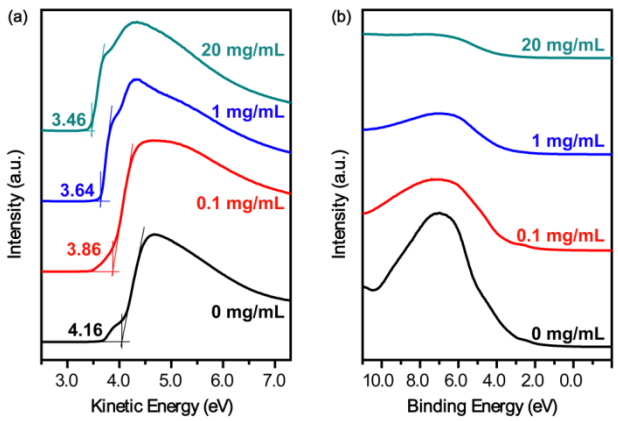

Figure 7 He I UPS spectra at (a) the low kinetic energy region and (b) the low binding energy region near the Fermi level for as-transferred and doped CVD graphene with various concentrations of *o*-MeO-DMBI solutions

The n-type doping effect of o-MeO-DMBI on graphene was also evaluated by photoelectron spectroscopy (PES) measurements. Figure 7 shows the ultraviolet photoelectron spectroscopy (UPS) spectra at the low kinetic energy region (Figure 7a) and valence band spectra at the low binding energy region (Figure 7b) for the as-transferred and doped CVD graphene with various concentrations of *o*-MeO-DMBI solutions. The vacuum level of CVD graphene when doped with different concentrations of *o*-MeO-DMBI solutions was measured by linear extrapolation of the low kinetic energy onset (secondary electron cutoff) of the UPS spectra. As shown in Figure 7a, with increasing solution concentrations, an obvious downward vacuum level shift of 0.7 eV was observed, i.e., the work function decreased from 4.16 eV for as-transferred CVD graphene to 3.46 eV for 20 mg/mL *o*-MeO-DMBI doped graphene, which further indicates that n-doped graphene films can serve as transparent conductive cathodes for OPV.

4 Single Walled Carbon Nanotube Sorting Process

The sorted HiPco single-walled carbon nanotubes (SWNTs) employed as part of the active layer of our solar cells are prone to defects during sonication and are difficult to align. Large-diameter Arc-discharged SWNTs are generally longer, straighter and have fewer defects due to their decreased wall curvature and hence are potentially better for charge transport. Therefore, we have been developing polymers to enable the sorting large-diameter Arc-discharged SWNTs (Wang *et al. ACS Nano 2013*). A

Dithiafulvalene/Thiophene (PDTFF-*m*T) polymer (Figure 8a) was found to be the most efficient polymer that selectively disperses semiconducting Arc-discharged SWNTs with a yield of more than 30%. The sorting process involves a rather simple sonication step followed by a centrifuge. From both the absorption spectroscopy (Figure 8a), and Raman spectroscopy measurement (Figure 8b), we observe a significant decrease in the first interband transition of metallic SWNTs (M11) peak for all the PDTFF-*m*T polymer dispersed SWNTs. We also fabricated thin film transistors (Figure 9a,b) with the polymer sorted SWNTs and recorded a maximum mobility of 2.8 cm^2/Vs and on/off ratio of 1.6 x 10^4 (Figure 9c). The sorted devices have an average on/off ratio of 1.56 ± 1.08 x 10^4 and an average mobility of 1.26 ± 0.51 cm^2/Vs, while the unsorted SWNT devices with the same tube density have a very low average on/off ratio of approximately 10 (Figure 9d), which is attributed to metallic SWNT pathways in the channel.

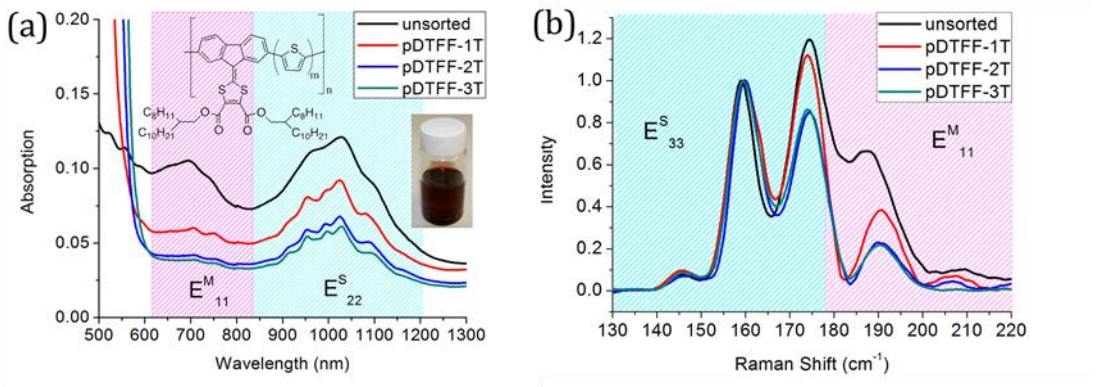

Figure 8 Optical absorption spectrum of carbon nanotubes before and after sorting with pDTFF-mT. The unsorted arc-discharged SWNTs were dispersed in N-Methyl-2-pyrrolidone. Inset: Chemical structure of poly(dithiafulvalene-fluorene-co-m-thiophene), A picture of a dispersion obtained from pDTFF-3T polymer; (b) Raman spectrum of unsorted and sorted SWNTs

We also investigated the sorting mechanism by increasing the ratio of thiophene to dithiafulvalene units in the polymer backbone (from pDTFF-1T to pDTFF-3T). We found that we could slightly improve the selectivity towards semiconducting SWNTs. This is likely due to the more flexible backbone of pDTFF-3T that allows the favorable wrapping of SWNTs with specific chirality as characterized by small-angle X-ray scattering. However, the dispersion yield was reduced from pDTFF-1T to pDTFF-3T. Molecular Dynamics simulations showed that the reduction is due to the smaller polymer/SWNT contact area, which reduces the dispersion ability of pDTFF-3T. We also predicted by Molecular dynamics simulations of

polymer backbone interactions with and without side chains that the presence of long alkyl side chains is responsible for the rise in the selectivity toward semiconducting tubes. This highlights the importance of the roles of the side chains to both solubilize and confer selectivity to the polymers.

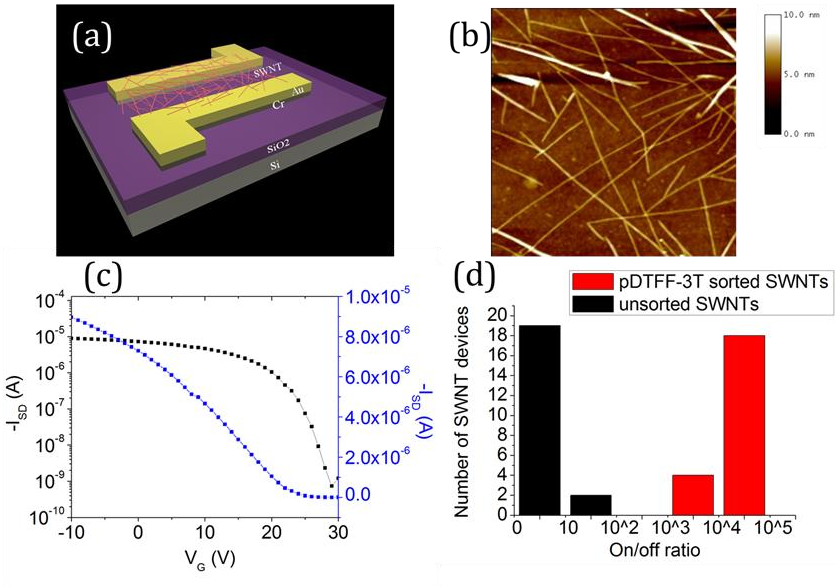

Figure 9. Electrical transport properties of thin film transistors made of pDTFF-3T-dispersed SWNTs in toluene. (a) Schematic diagram of device structure. (b) Morphology of SWNT films of ~30 SWNTs/μm^2. (c) Transfer curve of a typical device (V_{SD} = 1 V). (d) Histogram of on/off ratios for pDTFF-3T-sorted and unsorted SWNT devices of ~30 SWNTs/μm^2.

5 Summary

We summarize our work from the past year and our ongoing efforts towards an all carbon solar cell as follows:

1. We demonstrated the first all carbon solar cell consisting of a bilayer junction. The semiconducting HiPco SWNTs wrapped in P3DDT acted as the donor layer while the thermally evaporated fullerene C60 acted as the electron acceptor. The anode was formed out of reduced graphene oxide and the cathode consisted of n-type doped conductive SWNTs.

- The main limitations in the structure consisted of the short carrier diffusion length inherent of the adopted bilayer structure as well as the significant recombination losses due to the non-ideal energy level alignments.
- We are currently working on moving towards a bulk heterojunction to surpass our first limitation as well as adopting small diameter semiconducting SWNTs (CoMoCAT) which energy levels are better aligned with the C60.
- We are also working on fabricating smoother and more efficient n-type carbon based cathodes to be directly laminated on top of the solar cells.

2. We demonstrated that MoO_3can be used as an efficient and stable dopant of carbon nanotubes and graphene for transparent electrode applications.
    - However, the high activation temperature required hinders the direct application of this methodology onto flexible polymeric substrates. In addition, the SWNTs/MoO_3 composite is subject to degradation with oxidation at the high processing temperature
    - Our ongoing work focuses on the exploration of various other oxides as dopants as well as a range of inorganic materials with deep and shallow work function that can dope carbon materials either p or n-type.
3. We have also shown in a recent publication the use of an in-house made dopant *o*-MeO-DMBI to switch the behavior of CVD-grown graphene from p-type, to ambipolar and all the way to n-type. We demonstrated a change from a work function of 4.2 eV all the way to 3.5 eV indicating the viability of the material as a transparent cathode for organic solar cells.
4. Finally, a major focus has been the material processing of the SWNTs that can be employed as sensitizers in our solar cells. Our latest published efforts demonstrated the two step sorting process of large diameter semiconducting Arc-discharged SWNTs. These particular SWNTs absorb beyond 1500 nm and are ideal in multijunction solar cell applications.

Published Work

Hellstrom, S.L., Vosgueritchian, M., Stoltenberg, R.M., Irfan, I., Hammock, M., Wang, Y.B., Jia, C., Guo, X., Gao, Y., and Bao, Z. (2012). Strong and Stable Doping of Carbon Nanotubes and Graphene by MoOx for Transparent Electrodes. Nano Lett. *12*, 3574–3580.

Ramuz, M.P., Vosgueritchian, M., Wei, P., Wang, C., Gao, Y., Wu, Y., Chen, Y., and Bao, Z. (2012). Evaluation of Solution-Processable Carbon-Based Electrodes for All-Carbon Solar Cells. Acs Nano *6*, 10384–10395.

Wang, H., Mei, J., Liu, P., Schmidt, K., Jiménez-Osés, G., Osuna, S., Fang, L., Tassone, C.J., Zoombelt, A.P., Sokolov, A.N., et al. (2013). Scalable and Selective Dispersion of Semiconducting Arc-Discharged Carbon Nanotubes by Dithiafulvalene/Thiophene Copolymers for Thin Film Transistors. Acs Nano *7*, 2659–2668.

Wei, P., Liu, N., Lee, H.R., Adijanto, E., Ci, L., Naab, B.D., Zhong, J.Q., Park, J., Chen, W., Cui, Y., et al. (2013). Tuning the Dirac Point in CVD-Grown Graphene through Solution Processed n-Type Doping with 2-(2-Methoxyphenyl)-1,3-dimethyl-2,3-dihydro-1H-benzoimidazole. Nano Lett. in press.

Contacts

Zhenan Bao <zbao@stanford.edu>
Ghada Koleilat <ghadak@stanford.edu>